Published in final edited form as:
J Magn Reson Imaging. 2008 May ; 27(5): 1114–1121. doi:10.1002/jmri.21309.

Detection of Choline Signal in Human Breast Lesions with Chemical-Shift Imaging

Min-Ying L. Su

Abstract

Purpose—To investigate the application of MR spectroscopy using chemical-shift imaging (CSI) for characterizing human breast lesions at 1.5T, and to evaluate the diagnostic performance using the ROC (Receiver Operating Characteristics) analysis.

Materials and methods—Thirty-six patients (35−73 years old, mean 52), with 27 malignant and 9 benign lesions, underwent anatomical imaging, dynamic contrast-enhanced MR imaging, and CSI. The Choline (Cho) metabolite map was reconstructed from the multi-voxel CSI data. A mean Cho SNR was calculated for each lesion by averaging over Cho SNR's measured from all voxels that showed an identifiable Cho peak on the MRS spectra. The ROC analysis was performed, and the cutoff point yielding the highest accuracy was found to be Cho SNR > 3.2.

Results—The mean Cho SNR was 2.8 ± ? (range, 1.8 − 4.3) for the benign group, and 5.9 ± ? (2.1 − 17.5) for the malignant group (P = 0.02). Based on the criterion of Cho SNR >3.2 as malignant, CSI correctly diagnosed 22 of 27 malignant lesions and 7 of 9 benign lesions, resulting in the sensitivity of 81%, specificity of 78%, and overall accuracy of 81%. The 5 false-negative cases had small lesion size ranging from 1.0−2.0 cm. If the criterion was set higher at Cho SNR >4.0, the specificity was improved to 89%, but sensitivity was lowered to 67%. CSI corrected diagnosed two benign lesions that were mis-diagnosed as malignant based on the washout and plateau pattern in DCE enhancement kinetics.

Conclusion—CSI provided regional distribution of Cho, but was difficult to be interpreted to aid in diagnosis of breast cancer. The ROC analysis presented in this work could be used to set an objective diagnostic criterion depending on preferred emphasis on sensitivity or specificity.

Keywords

breast tumor diagnosis; chemical-shift imaging; choline-containing compounds; dynamic contrast-enhanced MRI; ROC analysis

INTRODUCTION

CONVENTIOANL DIAGNOSTIC METHOD SUCH AS X-ray mammography, ultrasound, and physical examination, each has limitations in the diagnosis of breast cancer. The American Cancer Society has recently issued a new guideline recommending annual screening MRI to women with an approximately 20−25% or greater lifetime risk of breast cancer (1). Preoperative MRI has become an established procedure for detecting multifocal or multicentric diseases to facilitate surgical planning, particularly in fibroglandular dense breasts (2). In a large series multi-center study, breast MRI of suspicious lesions performed prior to biopsy was shown to reach a high sensitivity of 88.1%, but with a relatively low specificity of 67.7% (3). Morphologic assessment (4,5) and kinetic analysis (6-8) could distinguish benign from malignant lesions. However, since not all malignant lesions showed the typical malignant morphologic or enhancement kinetic features (6,9-10); in order to reach a high sensitivity the specificity has to be compromised.

In vivo proton MR spectroscopy (MRS) is a non-invasive technique that can provide tumor metabolic information, which has been shown to have potential clinical applications in the diagnosis and management of patients with brain and prostate tumors (11,12). MRS has been increasingly applied for breast cancer studies in diagnosis and therapy response monitoring. Previous studies conducted at 1.5T have shown that in vivo single-voxel MRS can be used to distinguish between malignant and benign tissues based on the detection of choline (Cho) (e.g., detectibility or Cho signal to noise ratio (SNR)) (13-17). A pooled analysis of these five studies showed that MRS can reach to specificity to 85% (range, 67% − 100%). The addition of single-voxel MRS has been shown to improve the diagnostic specificity of dynamic contrast-enhanced (DCE) MR imaging (16,18). However, single-voxel technique has limitations in terms of lesion coverage, which may affect the sensitivity of Cho detection due to tumor heterogeneity.

On the other hand, multi-voxel techniques, chemical-shift imaging (CSI) or MR spectroscopic imaging (MRSI), may be used to acquire spectroscopic information from multiple voxels over a large volume of interest in a single measurement, hence suitable for analyzing the regional distribution of tumor metabolites. Although it is commonly used in the brain and prostate, only one feasibility study in 15 patients with breast lesions has been reported (19). The diagnostic accuracy of the MRSI was comparable with the results found in previous single-voxel MRS studies. Further investigations in larger studies are needed.

The present study applied CSI to detect Cho signal in 36 patients with biopsy-proven malignant (N=27) and benign (N=9) breast tumors. The purpose was two-fold, firstly to investigate the application of chemical-shift imaging for characterizing breast lesions using a clinical 1.5T scanner in a larger patient population, and secondly to evaluate the diagnostic performance of CSI using the ROC (Receiver Operating Characteristics) analysis.

MATERIALS AND METHODS

Patients

Thirty-six consecutive patients (range 35−73 years old, mean 52 years) enrolled from June 2004 to August 2005, who were scanned with the CSI MRS protocol were reported in this series. All patients had suspicious findings on physical examination, mammography, or sonography in the breast. They were referred to the study by medical or surgical oncologists. The inclusion criteria were patients who had suspicious lesions scheduled for biopsy, or who already had diagnosis of malignant breast lesions with needle-biopsy. Therefore, this is a selective patient group, not in a diagnostic setting. Only lesions greater than 1 cm were scanned with the CSI protocol and included in this study. Exclusion criteria were lesions smaller than 1 cm, or with presence of a breast hematoma adjacent to the suspicious lesion. This study was approved by the local institutional review board of the University of California-Irvine School of Medicine, and was HIPPA-compliant. The informed consent was obtained from each patient prior to the study.

The tissue diagnosis was obtained from the pathological report of the excision or needle biopsy. Of the 36 breast lesions evaluated, 27 (75%) were malignant and 9 (25%) were benign. Of the 27 malignant lesions, 20 were invasive ductal carcinomas, 4 were invasive lobular carcinomas, and the other 3 were mixed invasive ductal and lobular carcinomas. Of the 9 benign lesions, 6 were fibroadenomas, and 3 were fibrocystic changes.

MR Imaging and Chemical-Shift Imaging

All patients were examined with the same MRI/MRS protocol, which consisted of high-resolution imaging, dynamic contrast-enhanced MR imaging, and proton chemical-shift imaging. The studies were performed on a clinical 1.5T whole-body system (Eclipse; Philips

Medical System, Cleveland, Ohio) with the standard MRS acquisition software provided by the manufacturer. A body coil was used for transmission, and a dedicated four-channel phased-array breast coil (USA Instruments, Aurora, Ohio) was used for both MR imaging and MR spectroscopy. The coil was the original coil came with the scanner, designed to permit simultaneous imaging of both breasts. It did not allow for selective configuration of channels depending on the volume of interest.

All patients were examined in prone position, and the breasts were gently cushioned with rubber foam to reduce patient motion. After the localizer scan, sagittal view T_1-weighted pre-contrast images were acquired from the breast of concern, using a spin echo (SE) sequence with TR/TE 1000/12ms, matrix size 256×256, field of view (FOV) 22 cm, and 34 slices with 3−4 mm thickness. Following this, a 3D SPGR (RF-FAST) pulse sequence with 16 frames (repetitions) was prescribed for bilateral dynamic imaging. Thirty-two axial slices with 4 mm thickness were used to cover both breasts. The imaging parameters were TR/TE 10ms/3.6ms, flip angle 20°, acquisition matrix size 256×128, and FOV varying between 32 and 38 cm. The scan time was 42 seconds per acquisition. The sequence was repeated 16 times for dynamic acquisitions, 4 pre-contrast and 12 post-contrast sets. The contrast agent (Ominscan®, 1cc/10 lbs body weight) was manually injected at the beginning of the 5th acquisition, and was timed to finish in 12 seconds to make the bolus length consistent for all patients. Immediately following the contrast, 10 cc saline was used to flush the contrast medium.

The subtraction images were generated on the scanner console, by subtracting the pre-contrast images acquired in frame #3 from the 1-min post-contrast enhanced images acquired in frame #6. They were used for placing the volume of interest in the tumor for the MRS study. The CSI grid was carefully positioned to maximize coverage of the enhanced lesion on the subtraction images, as well as the hypointense lesion if it was visible on the sagittal pre-contrast T_1-weighted images. The point-resolved spectroscopic sequence (PRESS) sequence was used (20,21), and the parameters were: TR/TE = 1627/270 ms, matrix size = 8 × 8, FOV = 8 cm, and sagittal section thickness = 12mm. In order to improve the signal-to-noise, 4 acquisitions were taken and the total acquisition time was approximately 7 minutes. The resultant voxel size was $1.0 \times 1.0 \times 1.2\ cm^3$. The echo signal was digitized with 2048 data points and a spectral width of 2040 Hz. To improve field homogeneity over the CSI localization volume, a relatively large single voxel shimming (e.g., $10 \times 10 \times 10\ cm^3$) centering at the suspicious lesion was performed, and then these shim values were passed on to the CSI scans. The typical value for the water linewidth was usually 10−29 Hz (mean 20 Hz). The water suppression was accomplished with three chemical shift selective (CHESS) RF pulses (22,23) with a bandwidth of 64 Hz, and the fat signal was attenuated by using frequency-selective presaturation pulse (FATSAT).

MR and Spectroscopic Data Analysis

MRI data analysis was performed using our own analysis program written in Matlab (Version 6.5 for Windows, The MathWorks, Inc., MA) on a PC. The size of the lesion was measured based on contrast-enhanced images. The maximum intensity projection (MIP) of the axial subtraction images was generated, and the longest dimension and the perpendicular dimension were measured on the MIP. The number of slices the lesion covered was used to measure the third dimension.

For analysis of DCE kinetics, a region of interest (ROI) was drawn to cover the enhanced lesion based on the subtraction image at 1-min post contrast injection. The pre-contrast signal intensity was subtracted from the post-contrast signal intensity measured at each time point to obtain the signal enhancement time course. According to the MRI BI-RADS lexicon, the delayed phase in the time course was classified as persistent, plateau, or washout. Lesions with rapid

or medium initial enhancement followed by a delayed phase plateau or washout were classified as malignant. Lesions with the persistent enhancement time course were classified as benign.

The CSI raw data were reconstructed by Philips data analysis package (Philips Medical Systems, Cleveland, Ohio). The spectroscopic data were processed by Fourier transformation, with a Hamming filter in the spatial (phase-encoding) domains, Gaussian line broadening of 1.5 Hz, zero-filling to 4096 data points, and a high-pass filter (with Gaussian window width, 45 Hz) to reduce the residual water signal in the time domain. Phase and baseline corrections were manually done for each voxel. When the maximum peak of water was assigned to 4.7 ppm, typically the Cho peak was resolved at 3.22 ppm (range, 3.16 − 3.28 ppm) in breast tumors. The MR spectrum was further analyzed with great care by one spectroscopist when a Cho peak could be clearly identifiable above the baseline noise. The Cho peak area was quantified by employing the Levenberg-Marquardt algorithm to fit Gaussian to Lorenzian shape (24). After fitting, the peak height, width, area, and SNR were obtained. The SNR of Cho peak was calculated as the ratio of Cho peak height to the standard deviation of the baseline, which was measured in the flat noise baseline region (> 8 or < 0 ppm). For each patient a mean Cho SNR was calculated from all voxels that showed an identified Cho peak in the spectrum. For display, Cho metabolite map was linearly interpolated to 128 × 128 points. MATLAB software (Version 6.5 for Windows, The MathWorks, Inc., MA) was used for display of color-coded Cho metabolite maps.

Statistical Analysis

The histopathological diagnosis was used as the standard for evaluating diagnostic performance of DCE MRI and MRS. A receiver operating characteristic (ROC) curve was generated from the Cho SNR's measured from all 36 lesions. The cutoff point of the Cho SNR was determined as the value that yielded the highest accuracy, balancing between sensitivity and specificity (25). Then based on this cutoff Cho SNR as the criterion, the diagnostic accuracy, sensitivity, and specificity were calculated. The ROC analysis was performed using the MEDCALC® program (MediCal Software Inc., Belgium; version 9.3 for Windows).

An independent two-tailed, unequal variance *t*-test was employed to determine whether Cho SNR was different between malignant and benign lesion groups. A P-value < 0.05 was considered statistically significant. The t-test was performed by using a software package (version 6.0 for Windows; Origin, Microcal Software Inc., MA).

RESULTS

Lesion Characteristics

Based on the morphological pattern of enhancement, each lesion was categorized into one of these two groups according to the ACR BI-RADS lexicon: mass type lesion and non-mass type enhancements (26). Of the 27 patients with carcinoma, 19 (70%) presented a solitary mass or multiple differentiable masses with well-defined borders, and the other 8 (30%) showed non-mass enhancements without clearly defined borders. The median longest dimension of these solitary contrast-enhanced mass lesions measured on contrast-enhanced MRI was 4.0 cm (range, 1.2 − 9.4 cm). Of the 9 patients with benign lesions, 5 (56%) had mass lesions, with the median longest dimension of 1.3 cm (range, 1.0 − 1.7 cm), and 4 (44%) had non-mass lesions without clearly defined borders. The summary of patient age, tumor size, MR characteristics, and histopathological diagnosis of all 36 patients are listed in Table 1.

Dynamic Contrast Enhancement Imaging Results

The enhancement time course was categorized into one of three patterns according to the delayed phase: persistent, plateau, and washout. Of the 27 malignant cases, 20 (74%) showed

washout, 4 (15%) showed plateau, and 3 (11%) showed persistent enhancing pattern. Of the 9 benign cases, 7 (78%) exhibited persistent enhancement pattern, 1 (11%) showed plateau, and 1 (11%) showed washout. The washout and plateau patterns were considered suspicious of malignancy. Using the criteria, the diagnostic sensitivity and specificity based on contrast enhancement kinetics were 89% (24/27) and 78% (7/9), respectively.

Chemical-Shift Imaging Results

The diagnostic performance of Cho SNR measured by CSI was evaluated using the ROC analysis (Fig.1). The optimal Cho SNR cutoff point that yielded the highest accuracy was found to be > 3.2 (Fig. 1). On the basis of this criterion, a Cho SNR of greater than 3.2 was diagnosed as malignancy, whereas a Cho SNR of 3.2 or less was benignity. The resulted sensitivity was 81%, specificity was 78%, and the overall accuracy was 81%. There were 5 false-negative cases with Cho SNR from 2.1 to 3.2, including 4 invasive ductal carcinomas and one mixed invasive and lobular carcinoma. In 9 patients with benign lesions, seven were true-negative cases, including 4 fibroadenomas and 3 fibrocystic changes. The remaining two patients with fibroadenomas were false-positive cases, with Cho SNR of 4.0 and 4.3 (subject # 30 and 33 in Table 1). The mean Cho SNR was 2.8 (range, 1.8 − 4.3) for the benign group and 5.9 (2.1 − 17.5) for the malignant group (P = 0.02).

The diagnostic performance of CSI in all 12 lesions presenting non-mass type enhancements was evaluated. CSI correctly diagnosed all 8 malignant lesions, and 3 of 4 benign lesions, achieving an overall accuracy of 86%.

Example of CSI in One Malignant Lesion

Figure 2 demonstrates representative MR imaging and chemical-shift imaging from a 58-year-old patient (subject #2 in Table 1) with an invasive ductal carcinoma. The lesion had an irregular shape (Fig. 2a), and showed heterogeneous enhancements (Fig. 2b). Of a total of 64 CSI-voxels, 24 had identifiable Cho peaks. The mean ± standard deviation from these 24 voxels was 12.1 ± 7.4 (range, 2.8 − 26.6). A large range of Cho SNRs was noted. The metabolite map clearly demonstrated a regional Cho hot spot (Fig. 2c). The MR spectra obtained from 2×2 voxels (red outline) containing the Cho hot spot are shown in Fig. 2d. The Cho resonance peak is comprised of multiple choline-containing compounds (27-30). However, these signals cannot be resolved *in vivo* at 1.5T, and only a single resonance peak was observed. The signal enhancement time course from the tissues corresponding to the highest Cho voxel (Fig. 2d) showed the malignant pattern; with rapid enhancement during the initial phase followed by washout during the delayed phase (Fig. 2e).

Example of CSI in One Benign Lesion

Figure 3 shows MR imaging and chemical-shift imaging results from a 45-year-old patient (subject #33) with a benign fibroadenoma. This patient showed dense glandular tissues on the sagittal view pre-contrast image (Fig. 3a), and on the sagittal view subtraction image a heterogeneous enhancement area was noted in the anterior right breast (Fig. 3b). CSI demonstrated a regional Cho distribution in the enhanced areas (Fig. 3c). Ten CSI-voxels had identifiable Cho peaks. The mean ± standard deviation from these ten voxels was 4.3 ± 1.3 (range, 2.2 − 6.5). In Figure 3d, breast MR spectrum obtained from a voxel (red outline) showed an identifiable Cho peak. The signal enhancement time course corresponding to the Cho voxel (Fig. 3d) showed a benign pattern; with moderate enhancement during the initial phase followed by a persistent enhancement during the delayed phase (Fig. 3e).

DISCUSSION

Since human breast cancer is known to exhibit morphological and metabolic heterogeneity, multi-voxel MRS may be superior to the single-voxel technique for evaluating the spatial variation in cases presenting as a large heterogeneous lesion or multiple lesions. The incorporation of a CSI MRS sequence to the breast MR imaging protocol may provide metabolic information of the enhancing lesion shown on MRI. In our study CSI was performed using the PRESS sequence (20,21). The sequence with 4 averages took approximately 7 minutes. After including the additional time for voxel placement and shimming, the entire sequence can be completed within 15 minutes.

There was only one published paper reporting the use of CSI for diagnosis of breast cancer in 15 patients (19). One critical question to address is how to set the criteria for differentiating between malignant and benign lesions. We analyzed the CSI data using the ROC analysis, and set the criteria based on the optimal cutoff point to achieve the highest accuracy, as Cho SNR > 3.2. Using this criterion, the sensitivity, specificity, and accuracy were 81%, 78%, and 81%, respectively. They were in the same range as reported in previously published studies listed in Table 2. If we chose the same criteria (e.g., Cho SNR > 4) as used in Jacobs et al. (19), the specificity could be improved to 89%, but at the expense of compromised sensitivity (81% to 67%) and overall accuracy (81% to 72%).

Based on the criterion of Cho SNR > 3.2, there were 5 false negative cases. This might be due to partial volume effects from intermixed tumor and normal tissues in a voxel. In these five subjects, the tumor size in all 3 dimensions was relatively small, ranging from 1.0 − 2.0 cm. This was comparable to MRS voxel of $1.0 \times 1.0 \times 1.2\ cm^3$, thus very likely to suffer from the partial volume averaging effect. Due to this problem, CSI will have a very limited role for characterizing small lesions. On the other hand, among all 12 lesions presenting non-mass type enhancements, CSI correctly diagnosed all 8 malignant lesions and 3 of 4 benign lesions, with an overall accuracy of 86%.

The lipid contamination in CSI may also attribute to low sensitivity. The adipose tissue limits the ability to optimize the field homogeneity inside the selected volume, which in turn leads to broad resonance peaks and reduced SNR. Intense lipid resonances can also produce sideband artifacts. The detection of small Cho signals may be difficult because of overlaps with the wings or sidebands of the much larger residual water and lipid signals (31). The spectral quality may also be degraded by patient's respiratory motion (32).

We found two false-positive cases (subject #30 and 33) in our series. This has also been consistently reported in previous MRS studies. Kvistad et al. (14) and Yeung et al. (33) reported that Cho was present in isolated cases of fibroadenoma. In an ex vivo proton MRS study of fine-needle breast biopsy specimens, Mackinnon et al. (27) reported that three of the 15 fibroadenomas contained detectable levels of Cho. The study of Kvistad et al. (14) and Cecil et al. (34) found one case of fibrocystic disease, respectively. Roebuck et al. (35) reported one case of tubular adenoma. Therefore, these benign cases probably represent the actual limits of the specificity of breast MRS in diagnosis of breast cancer.

Previous in vivo MRS studies have demonstrated that elevated Cho peak at 3.2 ppm is observed in neoplastic tissues (14,33-35). High resolution proton-NMR spectra acquired from biopsy tissues have shown that a Cho resonance peak actually is comprised of multiple signals, such as phosphocholine, glycerophosphocholine, and free choline (27-30). Among these signals, the primary component contributing to the Cho peak is phosphocholine, a known precursor of cell membranes synthesis (36-40). Thus, the elevated Cho level in breast cancer may be associated with increased membrane synthesis by replicating cells. However, benign tissues such as proliferative fibroadenomas may also show a positive-Cho signal (14,27,33).

The high resolution and sufficient spatial coverage of the multi-voxel technique makes it advantageous over the single-voxel technique. However, a homogeneity field and improved water and lipid suppression is critically needed to detect a small Cho signal. Recently, Maril et al. (41) suggested that the combination of spatial saturation pulses and first-order shimming can provide an effective means to correct inhomogeneities in the breast. Quantitative measurement of Cho may improve the sensitivity of MRS, to minimize the impact due to variations in voxel size, adipose tissue content, and receiver coil efficiency. External or internal reference methods have been applied to quantify Cho levels in breast tissue at 1.5 T (42,43) and 4.0 T (44). These methods may be desirable for evaluating Cho concentration in breast lesions, but they require a long scan time to measure correction factors (e.g., receiver gain, partial volume effects, and T1 and T2 relation times, etc.), which can be done with the single-voxel technique, but not practical with the multi-voxel technique. Furthermore, a good reference scan and a good water and fat suppression is needed for quantification, which may not be achieved given the field inhomogeneity over the large CSI grid. Therefore, although quantitative MRSI is expected to provide a more accurate choline concentration, further technical improvements are needed to achieve this goal.

This was a relatively small series from a selective patient group. However, since the subjects were consecutive patients studied with this combined DCE and CSI protocol, it was still meaningful for analysis of diagnostic sensitivity and specificity of DCE MRI, only to be compared with CSI results. Of the 27 malignant lesions, the analysis of DCE enhancement time course showed 20 (74%) washout pattern, and 4 (15%) plateau pattern. The plateau pattern is considered equivocal, but is suspicious for recommending biopsy. In chemical-shift imaging, three of these four patients showed Cho SNR > 3.2, that were subsequently diagnosed as cancer. The other patient had Cho SNR of 3.2, and would be mis-diagnosed as benign on MRS. Three malignant lesions that showed persistent enhancing kinetics were mis-diagnosed as benign on DCE. Two of them had Cho SNR < 3.2, thus would also be mis-diagnosed as benign based on MRS. Therefore, CSI would not improve the sensitivity of DCE MRI.

Of the 9 benign lesions, there were two false positive findings based on DCE kinetics, which resulted in 78% specificity. One patient had the washout pattern and the other had the plateau pattern. Their Cho SNR were 2.9 and 2.7, respectively, thus they would be correctly diagnosed as benign based on the CSI criterion of SNR < 3.2. Therefore, consistent with previously published studies, the value of MR spectroscopy may lie on improving specificity of DCE MRI.

Jacobs et al (45) investigated the feasibility of combining DCE-MRI and MRSI in analyzing breast lesions. They reported that proton MRS appears to be a promising technique for classification of breast lesions when DCE results are equivocal. In our series, we had 5 cases with the equivocal plateau kinetics, MRS correctly diagnosed 3 malignant lesions and 1 benign lesion, but mis-diagnosed one malignant case as benign, therefore had an overall accuracy of 80%. The optimal analysis that can be performed is to directly compare whether the addition of multi-voxel MRSI can indeed improve the specificity, based on reading of experienced and inexperienced observers as reported in Meisamy et al. (18). This may be performed when more benign cases are available.

In summary, we demonstrated that the CSI technique can be incorporated into the clinical 1.5T breast MR imaging protocol within an acceptable scan time (approximately 15 min.). The multi-voxel MRS sequences are currently available on most clinical MR scanners. However, despite its wide application in brain and prostate tumor, these techniques were rarely applied for characterizing breast lesions. One major difficulty was how to interpret the Cho signal for diagnosis. The ROC analysis presented in this work can be used to set an objective diagnostic criterion depending on preferred emphasis on sensitivity or specificity. Since interpretation of

DCE MRI is set to reach a high sensitivity with compromised specificity, the metabolic information measured by CSI may be used for improving the specificity in diagnosis of breast tumors. However, its limitation in characterizing small lesions has to be considered. CSI may provide advantage over the single voxel technique for characterization of lesions presenting the non-mass type, diffuse enhancements.

REFERENCES

1. Saslow D, Boetes C, Burke W, et al. American Cancer Society Breast Cancer Advisory Group. American Cancer Society guidelines for breast screening with MRI as an adjunct to mammography. CA Cancer J Clin 2007;57:75–89. [PubMed: 17392385]
2. Sardanelli F, Giuseppetti GM, Panizza P, et al. Sensitivity of MRI versus mammography for detecting foci of multifocal, multicentric breast cancer in Fatty and dense breasts using the whole-breast pathologic examination as a gold standard. Am J Roentgenol 2004;183:1149–1157. [PubMed: 15385322]
3. Bluemke DA, Gatsonis CA, Chen MH, et al. Magnetic resonance imaging of the breast prior to biopsy. JAMA 2004;292:2735–2742. [PubMed: 15585733]
4. Nunes LW, Schnall MD, Orel SG, et al. Breast MR imaging: interpretation model. Radiology 1997;202:833–841. [PubMed: 9051042]
5. Nunes LW, Schnall MD, Orel SG. Update of breast MR imaging architectural interpretation model. Radiology 2001;219:484–494. [PubMed: 11323476]
6. Kuhl CK, Mielcareck P, Klaschik S, et al. Dynamic breast MR imaging: are signal intensity time course data useful for differential diagnosis of enhancing lesions? Radiology 1999;211:101–110. [PubMed: 10189459]
7. Wiener JI, Schilling KJ, Adami C, Obuchowski NA. Assessment of suspected breast cancer by MRI: a prospective clinical trial using a combined kinetic and morphologic analysis. Am J Roentgenol 2005;184:878–886. [PubMed: 15728612]
8. Fan X, Medved M, Karczmar GS, et al. Diagnosis of suspicious breast lesions using an empirical mathematical model for dynamic contrast-enhanced MRI. Magn Reson Imaging 2007;25:593–603. [PubMed: 17540270]
9. Weinstein D, Strano S, Cohen P, Fields S, Gomori JM, Degani H. Breast fibroadenoma: mapping of pathophysiologic features with three-time-point, contrast-enhanced MR imaging-pilot study. Radiology 1999;210:233–240. [PubMed: 9885614]
10. Wurdinger S, Kamprath S, Eschrich D, Schneider A, Kaiser WA. False-negative findings of malignant breast lesions on preoperative magnetic resonance mammography. Breast 2001;10:131–139. [PubMed: 14965573]
11. Leclerc X, Huisman T, Sorensen A. The potential of proton magnetic resonance spectroscopy (1H-MRS) in the diagnosis and management of patients with brain tumors. Current Opinion on Oncology 2002;14:292–298.
12. Kurhanewicz J, Vigneron DB, Nelson SJ. Three-dimensional magnetic resonance spectroscopic imaging of brain and prostate cancer. Neoplasia 2000;2:166–189. [PubMed: 10933075]
13. Jagannathan NR, Kumar M, Seenu V, Coshic O, Dwivedi SN, Julka PK, Srivastava A, Rath GK. Evaluation of total choline from in-vivo volume localized proton MR spectroscopy and its response to neoadjuvant chemotherapy in locally advanced breast cancer. Br J Cancer 2001;84:1016–1022. [PubMed: 11308247]
14. Kvistad KA, Bakken IJ, Gribbestad IS, Ehrnholm B, Lundgren S, Fjosne HE, haraldseth O. Characterization of neoplastic and normal human breast tissues with in vivo ^{1}H MR spectroscopy. J Magn Reson Imaging 1999;10:159–164. [PubMed: 10441019]
15. Tse GM, Ceung HS, Pang LM, Chu WC, Law BK, Kung FY, Yeung DK. Characterization of lesions of the breast with proton MR spectroscopy: comparison of carcinomas, benign lesions, and phyllodes tumors. Am J Roentgenol 2003;181:1267–1272. [PubMed: 14573418]
16. Huang W, Fisher PR, Dulaimy K, Tudorica LA, Ohea B, Mutton TM. Detection of breast malignancy: diagnostic MR protocol for improved specificity. Radiology 2004;232(2):585–591. [PubMed: 15205478]

17. Bartella L, Morris EA, Dershaw DD, Liberman L, Thakur SB, Moskowitz C, Guido J, Huang W. Proton MR spectroscopy with choline peak as malignancy marker improves positive predictive value for breast cancer diagnosis: preliminary study. Radiology 2006;239:686–692. [PubMed: 16603660]
18. Meisamy S, Bolan PJ, Baker EH, et al. Adding in vivo quantitative ^{1}H MR spectroscopy to improve diagnostic accuracy of breast MR imaging: preliminary results of observer performance study at 4.0T. Radiology 2005;236(2):465–475. [PubMed: 16040903]
19. Jacobs MA, Barker PB, DPhil, Bottomley PA, Bhujwalla Z, Bluemke DA. Proton magnetic resonance spectroscopic imaging of human breast cancer: a preliminary study. J Magn Reson Imaging 2004;19:68–75. [PubMed: 14696222]
20. Bottomley PA. Spatial localization in NMR spectroscopy in vivo. Ann. N.Y. Acad Sci 1987;508:333–348. [PubMed: 3326459]
21. Ordidge, RJ.; Bendall, MR.; Gordon, RE.; Connelly, A. Volume selection for in vivo spectroscopy.. In: Govil, G.; Khetrapal, CL.; Sarans, A., editors. Magnetic resonance in biology and medicine. Tata-McGraw-Hill; New Delhi, India: 1985. p. 387-397.
22. Hasse A, Frahm J, Hanicke W, Mattaei. ^{1}H NMR chemical shift selective (CHESS) imaging. Phys Med Biol 1985;30:431.
23. Doddrell DM, Galloway G, Brooks W, Filed J, Bulsing J, Irving M, Baddeley H. Water signal elimination in vivo, using suppression by mistimed echo and repetitive gradient episodes. J Magn Reson 1986;70:176–180.
24. Morr, JJ. The Levenberg-Marquardt algorithm implementation and theory, in Numerical Analysis, Ser. Lecture Notes in Mathemattics. Watson., G., editor. Springer-Verlag; New York: 1978. p. 105-116.
25. Le, CT. Introductory biostatistics. Wiley; Hoboken, NJ: 2003. Receiver operating characteristics curve.; p. 336-338.
26. American College of Radiology. ACR Breast Imaging Reporting and Data System, Breast Imaging Atlas. American College of Radiology; Reston, Va: 2003.
27. Mackinnon WB, Barry PA, Malycha PL, et al. Fine-needle biopsy specimens of benign breast lesions distinguished from invasive cancer ex vivo with proton MR spectroscopy. Radiology 1997;204:661–666. [PubMed: 9280241]
28. Cheng LL, Chang W, Smith BL, Gonzalez RG. Evaluating human breast ductal carcinomas with high-resolution magic-angle spinning proton magnetic resonance spectroscopy. J Magn Reson 1998;135:194–202. [PubMed: 9799694]
29. Gribbestad IS, Sitter B, Lundgren S, Krane J, Axelson D. Metabolite composition in breast tumors examined by proton nuclear magnetic resonance spectroscopy. Anticancer Res 1998;19:1737–1746. [PubMed: 10470108]
30. Sitter B, Sonnewald U, Spraul M, Fjosne HE, Gribbestad IS. High-resolution magic angle spinning MRS of breast cancer tissue. NMR Biomed 2002;15(5):327–337. [PubMed: 12203224]
31. Bolan PJ, DelaBarre L, Baker EH, Merkle H, Everson LI, Yee D, Garwood M. Eliminating spurious lipid sidebands in 1H MRS of breast lesions. Magn Reson Med 2002;48:215–222. [PubMed: 12210929]
32. Bolan PJ, Henry PierreGilles, Baker EH, Meisamy S, Garwood M. Measurement and correction of respiration-induced B_0 variations in breast 1H MRS at 4 Tesla. Magn Reson Med 2004;52:1239–1245. [PubMed: 15562472]
33. Yeung DK, Cheung HS, Tse GM. Human breast lesions: characterization with contrast-enhanced in vivo proton MR spectroscopy-initial results. Radiology 2001;220:40–60. [PubMed: 11425970]
34. Cecil KM, Schnall MD, Siegelman ES, Lenkinski RE. The evaluation of human breast lesions with magnetic resonance imaging and proton magnetic resonance spectroscopy. Breast Cancer Res Treat 2001;68:45–54. [PubMed: 11678308]
35. Roebuck JR, Cecil KM, Schnall MD, Lenkinski RE. Human breast lesions: characterization with proton MR spectroscopy. Radiology 1998;209:269–275. [PubMed: 9769842]
36. Gribbestad IS, Singstad TE, Nilsen G, Fjosne HE, Engan T, Haugen OA, Rinck PA. In vitro proton NMR spectroscopy of extracts from human breast-tumors and noninvolved breast tissue. Anticancer Res 1993;13:1973–1980. [PubMed: 8297103]

37. Gribbestad IS, Petersen SB, Fjosne HE, Kvinnsland S, Krane J. H-1 NMR spectroscopic characterization of perchloric acid extracts from breast carcinomas and noninvolved breast tissue. NMR Biomed 1994;7:181–194. [PubMed: 7946996]

38. Ting YT, Sherr D, Degani H. Variations in energy and phospholipid metabolism in normal and cancer human mammary epithelial cells. Anticancer Res 1996;16:1381–1388. [PubMed: 8694505]

39. Katz-Brull R, Margalit R, Degani H. Differential routing of choline in implanted breast cancer and normal organs. Magn Reson Med 1996;46:31–38. [PubMed: 11443708]

40. Aboagye EO, Bhujwalla ZM. Malignant transformation alters membrane choline phospholipids metabolism of human mammary epithelial cells. Cancer Res 1999;59:80–84. [PubMed: 9892190]

41. Maril N, Collins CM, Greenman RL, Lenkinski RE. Strategies for shimming the breast. Magn Reson Med 2005;54:1139–1145. [PubMed: 16217775]

42. Bakken IJ, Gribbestad IS, Singstad TE, Kvistad KA. External standard method for the in vivo quantification of choline-containing compounds in breast tumors by proton MR spectroscopy at 1.5 Tesla. Magn Reson Med 2001;46:189–192. [PubMed: 11443726]

43. Baik HM, Su MY, Yu Hon, Mehta R, Nalcioglu O. Quantification of choline-containing compounds in malignant breast tumors by 1H MR spectroscopy using water as an internal reference at 1.5T. Magn Reson Mater Phy 2006;19:96–104.

44. Bolan PJ, Meisamy S, Baker EH, Lin J, Emory T, Nelson M, Everson LI, Yee D, Garwood M. In vivo quantification of choline compounds in the breast with ^{1}H MR Spectroscopy. Magn Reson Med 2003;50:1134–1143. [PubMed: 14648561]

45. Jacobs MA, Barker PB, DPhil, Argani P, Ouwerkerk R, Bhujwalla ZM, Bluemke DA. Combined dynamic contrast enhanced breast MR and proton spectroscopic imaging. J Magn Reson Imaging 2005;21:23–28. [PubMed: 15611934]

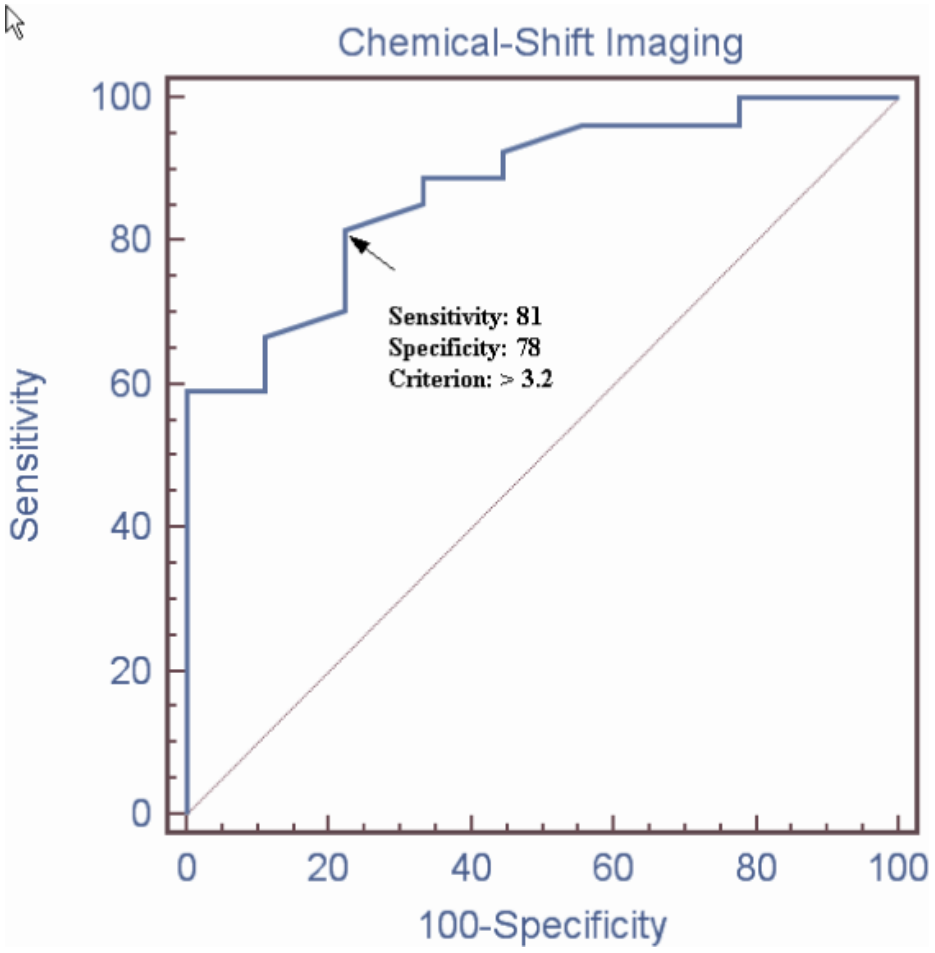

Figure 1.
The ROC curve generated from the Cho SNR measured in the 36 lesions (27 malignant and 9 benign). With a Cho SNR cutoff point of > 3.2 as malignancy, the overall accuracy was 81%; with a sensitivity of 81% and a specificity of 78%.

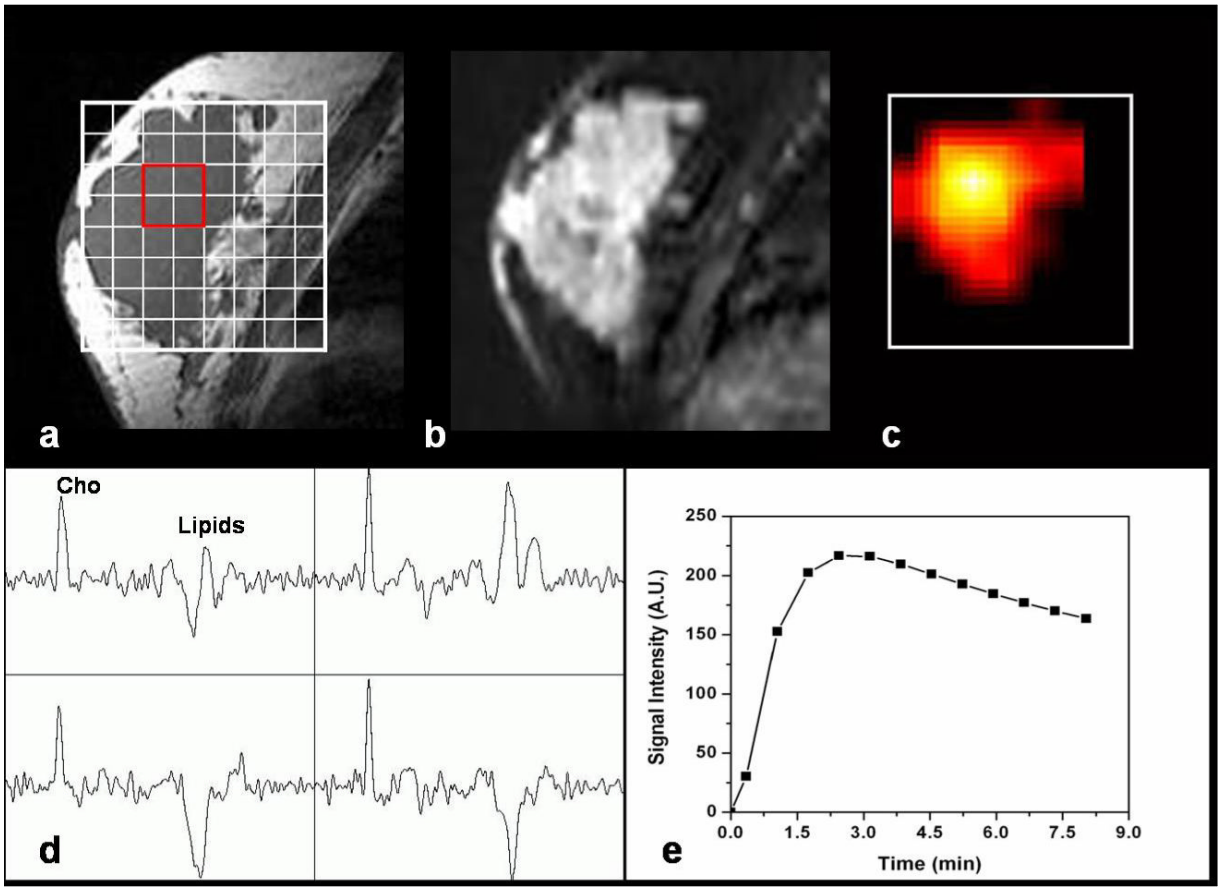

Figure 2.

MR imaging and chemical-shift imaging from a 58-year-old patient (#2) with an invasive ductal carcinoma. (a) The sagittal T_1-weighted pre-contrast MR image shows one large lesion with hypointense signal. (b) Heterogeneous signal intensity is shown on the sagittal view enhancement map. This image was reformatted from the axial subtraction images, thus had a low spatial resolution. (c) The metabolite map demonstrates a regional Cho distribution on the sagittal pre-contrast MR image. (d) Breast MR spectra obtained from 2×2 voxels (red outline) in the center of the tumor show high Cho peaks (mean SNR = 22.4). (e) The signal enhancement time course measured from tissues corresponding to the highest Cho voxel shows the malignant pattern with washout during the delayed phase.

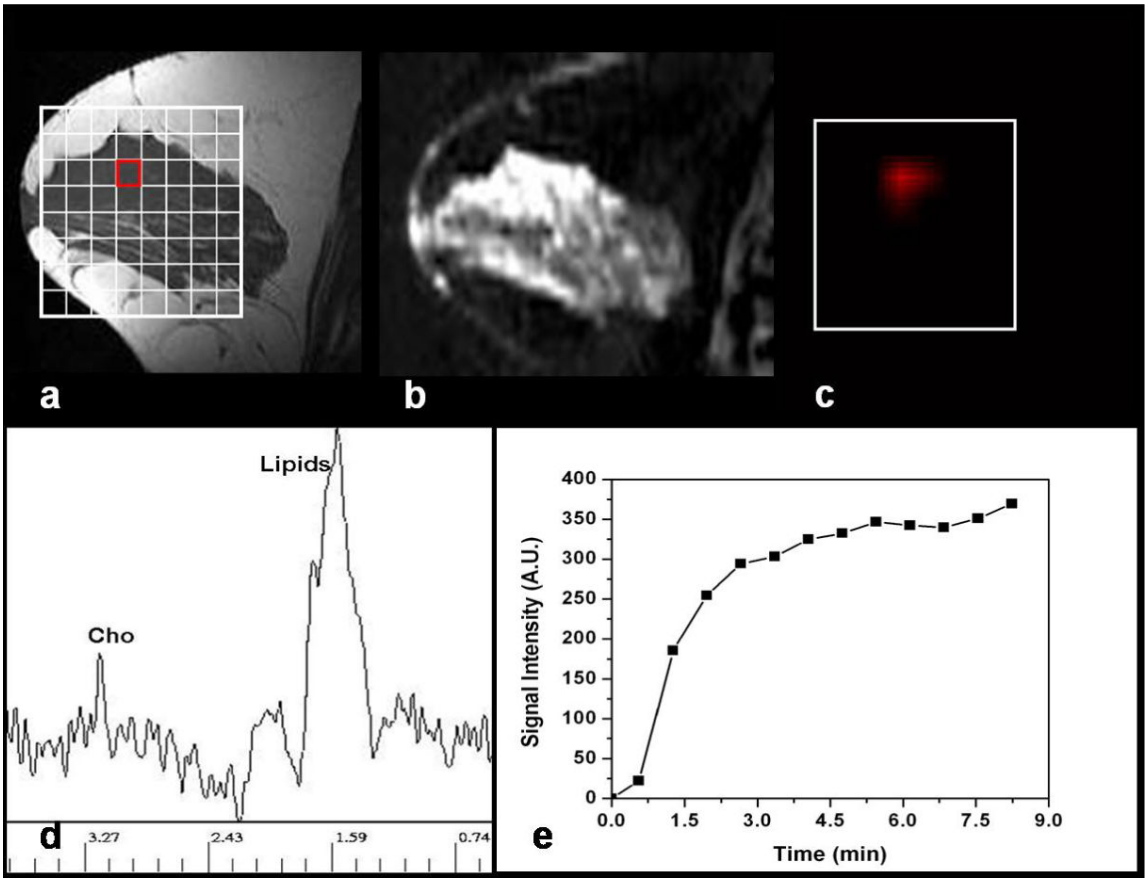

Figure 3.

MR imaging and chemical-shift imaging from a 45-year-old patient (#33) with benign fibroadenoma. (a) The sagittal T_1-weighted pre-contrast MR image shows very dense glandular tissues in the right breast. (b) The sagittal view enhancement map shows a heterogeneously enhanced area in the anterior right breast. (c) The Cho metabolite map demonstrates elevated signal in the enhanced lesion. (d) MR spectrum from a voxel (red outline) clearly demonstrates a Cho peak, with Cho SNR = 6.5. (e) The signal enhancement time course from tissues corresponding to the Cho voxel shows the benign pattern with persistent enhancements during the delayed phase.

Table 1

Summary of patient age, tumor size, MR characteristics, and histopathological diagnosis

Patient No.	Age (yrs)	*Tumor Size (mm)	DCE kinetic pattern	Histopathologic Finding	Cho SNR
1	35	70×59×84	plateau	IDC	7.5
2	58	60×40×95	washout	IDC	12.1
3	49	21×19×24	washout	IDC	9.1
4	68	40×22×40	washout	IDC	6.0
5	43	Non-Mass	washout	ILC	4.0
6	37	25×25×35	washout	IDC	6.4
7	51	Non-Mass	plateau	ILC	3.6
8	54	30×46×20	washout	IDC	8.7
9	49	Non-Mass	washout	IDC	7.1
10	46	Non-Mass	washout	IDC	6.9
11	50	Non-Mass	washout	IDC + ILC	4.4
12	53	40×16×28	washout	IDC	7.0
13	51	53×33×59	washout	IDC	6.7
14	51	Non-Mass	washout	IDC	4.9
15	46	36×32×60	plateau	IDC	17.5
16	45	85×50×56	washout	IDC	9.3
17	59	34×20×32	washout	IDC	4.2
18	65	30×20×35	washout	ILC	5.3
19	41	33×30×22	washout	IDC + ILC	4.6
20	47	Non-Mass	washout	IDC	4.2
21	46	14×10×10	washout	IDC	2.8
22	62	15×15×16	washout	IDC	3.4
23	63	10×10×12	persistent	IDC	2.1
24	59	15×15×20	plateau	IDC + ILC	3.2
25	69	11×11×20	washout	IDC	3.0
26	58	10×10×12	persistent	IDC	2.7
27	73	Non-Mass	persistent	ILC	3.4
28	46	10×10×10	plateau	Fibrocystic changes	2.7
29	47	Non-Mass	persistent	Fibroadenoma	3.2
30	48	12×12×12	persistent	Fibroadenoma	4.0
31	46	10×10×12	washout	Fibroadenoma	2.9
32	47	Non-Mass	persistent	Fibrocystic changes	2.4
33	45	Non-Mass	persistent	Fibroadenoma	4.3
34	50	12×10×10	persistent	Fibroadenoma	2.0
35	50	Non-Mass	persistent	Fibrocystic changes	1.8
36	45	12×1.5×1.6	persistent	Fibroadenoma	2.4

Note. IDC = invasive ductal carcinoma, ILC = invasive lobular carcinoma

*Tumor size estimated on contrast-enhanced MRI.

Table 2

Summary of sensitivity and specificity in breast lesion diagnosis using in vivo MR spectroscopy

MR Study (Reference Number)	*No. of Lesions (M/B)	Sensitivity (%)	Specificity (%)	‡Cho detection criterion	†MR Spectroscopy Tool
Jagannathan et al. (13)	46(32/14)	81	86	Presence, or not	SV
Kvistad et al. (14)	22(11/11)	82	82	Presence, or not	SV
Tse et al. (15)	40(19/21)	89	100	Cho SNR ≥ 2	SV
Huang et al (16)	30(18/12)	100	67	Cho SNR ≥ 2	SV
Bartella et al. (17)	57(31/26)	100	88	Cho SNR ≥ 2	SV
Jacobs et al. (19)	18(8/7)	87	85	Cho SNR ≥ 4	CSI

Note.

*No. of Lesions (/) = total lesions (malignant/benign).

‡Cho detection criterion; Cho SNR = Choline signal-to-noise ratio.

†MRS technique; SV = single-voxel spectroscopy, CSI = chemical-shift imaging.